Multi-sensing platform design with a grating-based nanostructure on a coverslip substrate

J.J. Imas[1,2], Ignacio Del Villar[1,2], Carlos R. Zamarreño[1,2], Subhas C. Mukhopadhyay[3,] and Ignacio R. Matías[1,2,*]

[1] Department of Electrical, Electronics and Communications Engineering, Public University of Navarra, 31006 Pamplona, Navarra, Spain
[2] Institute of Smart Cities, Public University of Navarra, 31006 Pamplona, Navarra, Spain
[3] School of Engineering, Macquarie University, Sydney, NSW 2109, Australia

*natxo@unavarra.es

Abstract. Two different thin film designs with a grating pattern are simulated on a soda lime coverslip, which acts as optical waveguide, with the purpose of generating both a lossy mode resonance (LMR) in transmission and reflection bands. This way both phenomena can be made sensitive to different parameters, leading to a multi-sensing device. The first design consists of a grating patterned in a SnO_2 thin film deposited on the coverslip. The performance of the device in both transmission and reflection is numerically studied in air for different values of the grating pitch. Small grating pitches (in the order of the μm) are more suitable for generating the reflection bands while larger values (500 μm or more) are required to produce the LMR, when the reflection bands are no longer visible. Due to the inability to obtain both phenomena with this design, a second design is assessed, where the grating is combined with a section of constant thickness. In this case the desired response is obtained, which opens the path to use this device for multi-sensing applications, measuring several parameters at the same time.

Keywords: Sensor, lossy mode resonance (LMR), coverslip, gratings, waveguides

1 Introduction

Lossy mode resonances (LMRs) occur when the real part of the permittivity of the thin film material is positive and higher in absolute value than its imaginary part and both the real part of the permittivity of the optical waveguide and the surrounding medium. Metal oxides and polymers are the materials that fulfil these conditions [1]. LMR based sensors have multiple applications including refractive index sensing, gas detection, humidity sensing, pH sensing or biosensing [1–3], where the waveguide is usually an optical fiber.

However, in recent years, LMRs have also been obtained employing planar waveguides (glass slides, coverslips). Their main advantage over optical fibers is that they are more

robust and cost-effective. In addition, only a polarizer is needed in the case of planar waveguides, as opposed to optical fibers, where both an inline polarizer and a polarization controller are required to properly tune the polarization state of light [4].
Different sensors have been developed based on planar waveguides, most of the times measuring two parameters at the same time as in [5] (refractive index and temperature), [6] (temperature and humidity), or [7] (refractive index in two different liquids). This is achieved by depositing two thin films with different thicknesses on the same side [5,7] or on both sides [6] of the planar waveguide. The thicknesses have to be carefully chosen so that both resonances are in the wavelength range under study but far enough so they do not overlap.
Following this tendency of developing multi-sensing platforms based on planar waveguides and LMRs, the purpose of this work is to explore, by means of theoretical simulations, the possibility of introducing a grating pattern on a thin film deposited on a coverslip. This way, the thin film will produce the LMR in the transmission spectrum while the grating pattern will generate bands in the reflection spectrum. Each of these phenomena could be employed to measure a different parameter. In the first place, a design consisting of a pure grating pattern is assessed, and then, the combination of a grating pattern and a section of constant thickness is analyzed.

2 Theory and simulations

The structure under study is a soda-lime coverslip on which a SnO_2 thin film is deposited and different thin film patterns are considered. The material employed for the films is SnO_2, which fulfils the conditions for generating LMRs [1,8]. Two different designs have been studied, whose results are shown in the following section: a grating pattern with a 50% duty cycle (only half of each pitch is covered by the thin film) and the combination of a grating pattern with a section of constant thickness. Two possibilities have been considered for a subsequent practical implementation: photolithography and a focused ion beam scanning electron microscope (FIB-SEM).
A schematic representation of the two structures that are simulated, as well as a close-up of the section and the top-view of the grating pattern are shown in Fig. 1. Regarding the section, the thin film has a thickness of 160 nm (this choice will be explained afterwards) while the coverslip and the poly(methyl methacrylate) (PMMA) substrate have a thickness of 150 μm and 5 mm, respectively. The coverslip acts as the optical waveguide, and the role of the PMMA substrate is to support the structure. A total length of 20 mm is considered, which is a standard value for a coverslip.

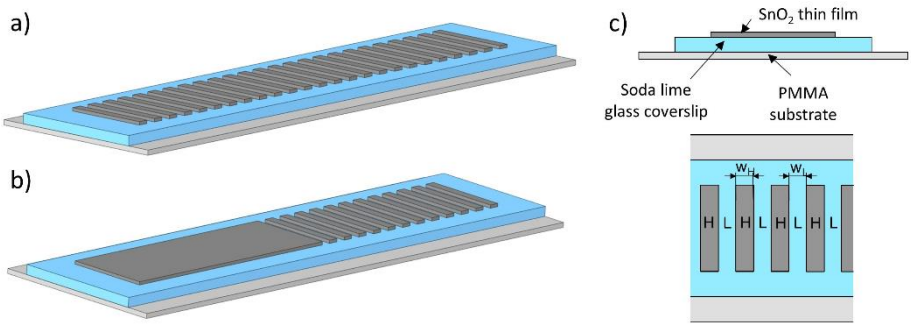

Fig. 1. a) 3D schematic diagram of a coverslip with a grating pattern on a thin film. b) Same as a) for a coverslip with a thin film with a section of constant thickness and a section with a grating pattern. c) Section of the coverslip and top view of the gratings.

The gratings patterned on the thin films are known as Bragg gratings [9,10] (other names are also used such as Bragg stacks [11], multilayer stacks [12,13], or micro-gratings [14]) and they produce bands in the reflection spectrum whose central wavelength is given by the Bragg-Snell equation for normal incidence:

$$m\lambda = 2\left(n_{effH}w_H + n_{effL}w_L\right) \quad (1)$$

where m is the diffraction order and n_{effH}, n_{effL}, w_H and w_L are the effective refractive indices and widths of the sections with the high- (H) and low- (L) refractive index materials respectively. As it has be decided to employ a 50% duty, $w_H = w_L$.
In the structures under study, n_{effH} and n_{effL} correspond to the effective refractive index of the sections with and without thin film, respectively. Nevertheless, the SnO_2 thin film does not appreciably affect the effective refractive index of the corresponding section. Therefore, it can be considered that $n_{effH} = n_{effL} = n_{eff}$, where n_{eff} is defined as the effective refractive index of the structure. If it is considered that the addition of w_H and w_L is equal to the pitch of the grating (Λ), then Eq. (1) can be simplified in our case to:

$$m\lambda = 2n_{effH}\Lambda \quad (2)$$

The structures studied in this work were analyzed with the commercial software FIMMWAVE. The propagation was calculated with FIMMPROP, a module integrated with FIMMWAVE. For the section, a non-uniform mesh of 500 elements was used in the Y direction. In the case of the PMMA substrate, only a thickness of 30 µm is considered in the simulation (as stated above, it only supports the structure, not affecting the propagation of light, so it is not necessary to consider the total thickness of this layer). The non-uniform mesh is used in the Y direction because the SnO_2 thin film is much thinner than the rest of the layers. With respect to the X direction, only one element is required in the mesh as the program establishes that there are not going to be changes in power along the X axis.

Regarding the materials, for the SnO_2 thin film, a refractive index of 1.9 + 0.01i was used based on ellipsometric measurements in [15]. The coverslip is made of soda lime glass, whose refractive index model was taken from [16], while the model for PMMA is obtained from [17]. The surrounding medium refractive index (SRI) is equal to 1 (air).

A schematic diagram of the setup that will be used for interrogating the structures under study is depicted in Fig. 2, in which it will be required to measure both the reflection and the transmission spectra. A halogen light source (for example, TAKHI Halogen source, from Pyroistech S.L., was employed in [5]) will be connected to input 1 of an optical circulator (for instance, WMC3L1S from Thorlabs). One end of the device under study will be connected to output 2 of the optical circulator and the other end will be connected to a spectrometer to measure the transmitted power (such as a NIRQuest NIR spectrometer, from OceanOptics). A linear polarizer (LPVIS050 from Thorlabs was used in [5]) will be placed between the output of the optical fiber that couples the light into the coverslip and the coverslip itself [6] to control the polarization state of light. Output 3 of the optical circulator will be connected to another spectrometer in order to measure the reflected power. All the connections are made with multimode optical fibers.

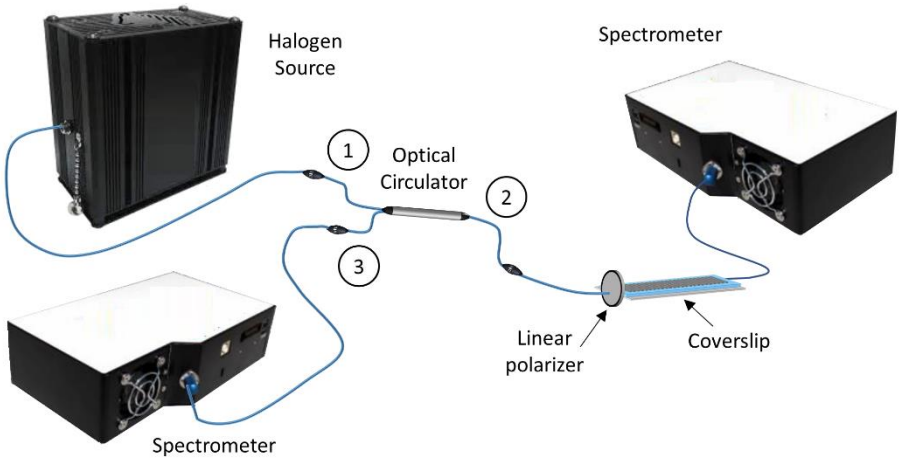

Fig. 2. Schematic of the setup that would be required for the interrogation of the device.

3 Results

3.1 Grating pattern

In the first place, the structure consisting of a coverslip with a SnO_2 grating pattern on top of it was studied. Different grating pitch values, from 4 μm to 20,000 μm, were assessed, keeping in all cases a total length of 20 mm. Therefore, the number of periods

varies from 500 (4 µm grating period) down to 1 (20,000 µm). The thickness of the SnO_2 thin film is 160 nm so the LMR is centered in the studied wavelength range (1200 - 1800 nm). Transverse electric (TE) polarized light is employed. It has been decided to use TE polarization as it gives better results than transverse magnetic (TM) polarization in the case of the D-shaped optical fiber for the same thin film design [18].
The transmitted power for each simulated value of the grating pitch is shown in Fig. 3. In all the cases, the transmission spectrum has been obtained after subtracting the transmitted power corresponding to the blank device (coverslip with a length of 20 mm and no thin film). It can be appreciated that, with the lowest pitch values (4 µm, 8 µm, and 10 µm), no resonance appears. If the grating pitch is increased by one order of magnitude (50 µm, 80 µm, and 100 µm cases), it seems that a resonance starts to appear, but it still is not very clear. It is required to increase the pitch another order of magnitude (500 µm, 800 µm) to clearly see the generation of an LMR. If the grating pitch is further increased (20,000 µm; which corresponds to only one period and can be hardly considered a grating), the LMR gains in definition, and it can be observed that it has shifted to the red in comparison with the previous cases.

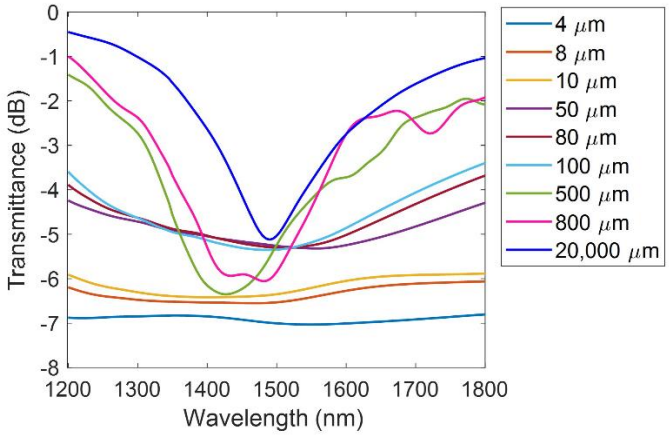

Fig. 3. Transmitted power for different values of the grating pitch (from 4 µm to 20,000 µm) over a total grating length of 20 mm.

Regarding the reflection bands, Table 1 includes their expected position using Eq. (2) and the ones obtained with the simulations (represented in Fig. 4a) for grating pitch values of 4, 8 and 10 µm, and it can be checked that they are very similar. The theoretical positions of the reflection bands have been calculated using n_{eff} = 1.508 in Eq. (2), which is the average refractive index value of soda lime glass in the studied range (from 1200 nm to 1800 nm) [16], as the effective index of the structure will be close to this value. For the sake of simplicity, only the values that belong to the studied wavelength range are shown in the table.

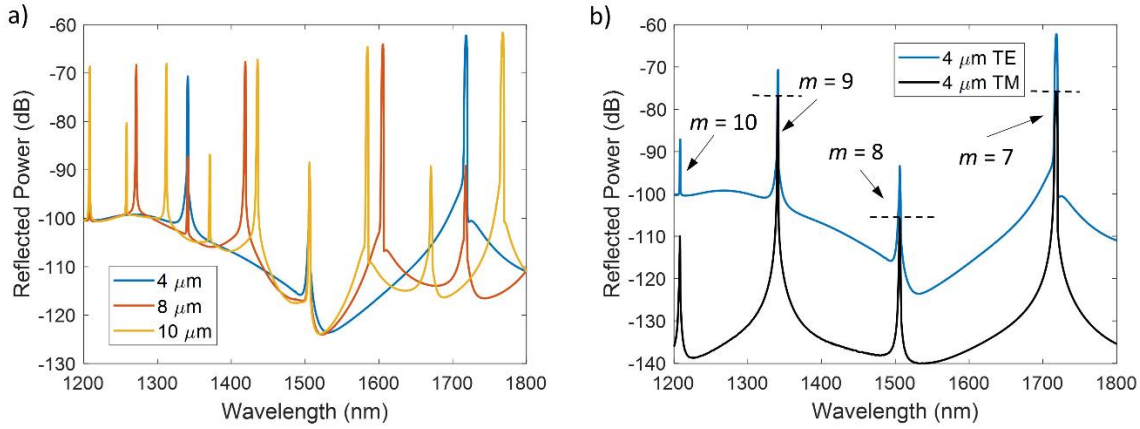

Fig. 4. Reflection bands for different values of the grating pitch a) Results for a pitch of 4 μm, 8 μm, and 10 μm (TE polarization in all cases) b) Results for a pitch of 4 μm for both TE and TM polarization.

Table 1. Theoretical and simulated wavelengths for the reflection bands for different values of the grating pitch.

	Theoretical wavelengths from formula (nm)			Wavelengths obtained in simulation (nm)		
	Pitch			Pitch		
m	4 μm	8 μm	10 μm	4 μm	8 μm	10 μm
7	1723			1718		
8	1508			1506		
9	1340			1341		
10	1206			1208		
11-13						
14		1723			1717	
15		1609			1605	
16		1508			1506	
17		1419	1774		1419	1768
18		1340	1676		1341	1671
19		1270	1587		1271	1584
20		1206	1508		1208	1506
21			1436			1435
22			1371			1371
23			1311			1312
24			1257			1258
25			1206			1208

It can also be checked in Fig. 4b, where the results for a grating pitch of 4 μm are represented for both TE and TM polarization, that the reflection bands reach a higher intensity in the TE polarized case, as it was expected (the dashed lines in Fig. 4b indicate the position of the maximum in the TM bands). All the other cases that are shown in this work correspond to TE polarization.

On the other hand, it can be observed both in Fig. 4a, and Fig. 4b that the reflected power of the bands with odd *m* is higher than that of the bands with even *m* (their values are indicated for the 4 μm grating pitch in Fig. 4b and the values of *m* for the 8 μm, 10 μm cases in Fig. 4a are included in Table 1). For instance, in the case of the 4 μm grating pitch, the reflection bands at 1718 nm ($m = 7$) and 1341 nm ($m = 9$) have a higher intensity than the ones at 1506 nm ($m = 8$) and 1208 nm ($m = 10$). These last two bands can be seen in Fig. 4b, but not in Fig. 4a, where they are hidden by more intense reflection bands corresponding to other values of the grating pitch.

However, considering this distinction between bands with odd and even *m*, there are no relevant differences among the bands corresponding to different values of the grating pitch in Fig. 4a (peak values of around -70 dB for odd *m* values and -90 dB for even *m* values).

If the grating pitch is increased up to 50 μm (see Fig. 5), more reflection bands are obtained in the same wavelength range, simply due to Eq. (2). Obviously, these reflection bands are closer to each other in comparison with the previously shown cases for lower grating pitch values. It can still be appreciated the difference in power between the bands with odd and even *m* (although this difference is less important at shorter wavelengths). Similar results (not shown for the sake of clarity) are obtained for 80 μm, and 100 μm (cases studied in in Fig. 3).

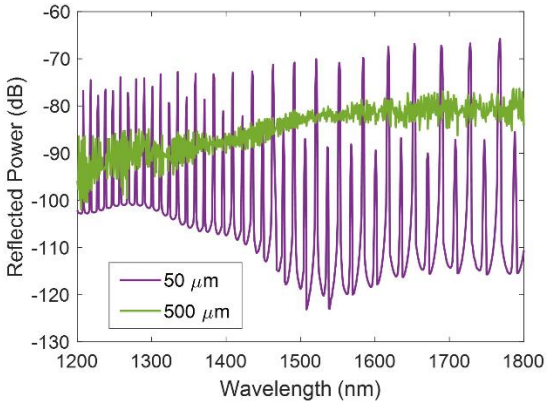

Fig. 5. Reflection bands for different values of the grating pitch (50 μm, 500 μm).

If the grating pitch is further increased to 500 μm (see again Fig. 5), the reflection bands are so close to each other that they are no longer distinguishable with the employed resolution. It must be considered that it was necessary to use this value for the grating pitch in order to generate an LMR (see Fig. 3). The same result (no reflection bands) is obtained for the remaining grating pitch values (800 μm, 20,000 μm) that have been studied in transmission.

The main conclusion for this device is that a value of the grating pitch that is suitable for generating the LMR (500 µm or higher), is not adequate for generating the reflection bands (they get too close to each other). On the other hand, when the reflection bands are clearly distinguishable (for instance, with a grating pitch in the order of the few µm), there is no LMR in transmission.

3.2 Grating pattern with a constant thickness section

The easiest option to solve the problems from the previous design seems to substitute a part of the grating by a section of constant thickness (see Fig. 1b). This way, the grating section (with a grating pitch in the order of the few µm) can produce the reflection bands, while the section of constant thickness generates the LMR. As in the previous case, TE polarization is used, the SnO_2 thin film thickness is 160 nm and the surrounding medium is air. The length of both sections (grating and section of constant thickness) is 10 mm, and three cases have studied: grating pitch of 4 µm (2500 periods), 8 µm (1250 periods) and 10 µm (1000 periods). The transmission spectrum and the reflection bands are shown in Fig. 6a, and Fig. 6b respectively.

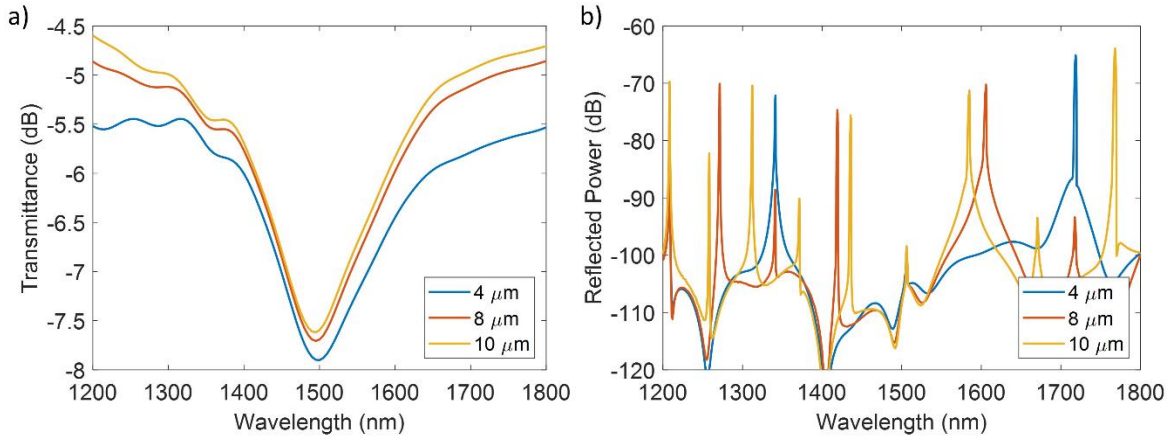

Fig. 6. Coverslip with a thin film with a section of constant thickness and a section with a grating pattern. a) Transmission spectrum for pitch values of 4 µm, 8 µm, and 10 µm. b) Reflection bands for pitch values of 4 µm, 8 µm, and 10 µm.

It can be observed that the desired response is obtained, that is, bands appear in the reflection spectrum due to the gratings and an LMR is generated in transmission thanks to the section of constant thickness. The position of the reflection bands is the same as in the previous device (see again Table 1 and Fig. 4a), which means we can still use Eq. (2). Comparing Fig. 6b with Fig. 4a, it can also be appreciated that the reflection bands in Fig. 6b are less intense when approaching 1500 nm due to the presence of the LMR at that wavelength. The reflection bands located at 1500 nm lose around 10 dB in Fig. 6b with respect to Fig. 4a, but the ones at around 1400 nm and 1600 nm also lose around 5 dB.

Nevertheless, even if the initial purpose has been achieved, it has to be considered that the LMR resonances are not very deep and the reflection bands are not very strong. The LMR resonance depth is in the range from 2.5 to 3 dB depending on the value of the pitch and the highest reflection bands achieve values around -70 dB, which are not very suitable for a practical implementation of this device. Different possibilities, including modifying the dimensions of the coverslip or employing other materials, could be explored in order to improve the response of the device.

4 Conclusions

Two different structures, both based on employing a coverslip as optical waveguide, have been theoretically studied in this work. The first one consisted on a grating pattern inscribed on a SnO_2 thin film deposited on the coverslip. It has been demonstrated that it is not possible to find a suitable value of the grating pitch for this design to produce both an LMR in transmission and reflection bands. This problem has been solved with the second design, which combines the grating with a section of constant thickness, generating both the LMR and the reflection bands.
The next step will be to manufacture this structure by means of a FIB-SEM or a photolithography process, although it is interesting to try to optimize the performance of the device in the first place, managing to obtain a deeper LMR and more intense reflection bands. Then, once the device has been fabricated the response of the LMR and the reflection bands should be characterized for two different parameters (for instance, the SRI and the temperature), opening the door to the development of a multi-sensing platform.

Acknowledgments

This research was funded by the Spanish Ministry of Universities (FPU18/03087 grant), and the Spanish Ministry of Economy and Competitiveness (PID2019-106231RB-I00 research fund).

References

1. Del Villar, I.; Arregui, F.J.; Zamarreño, C.R.; Corres, J.M.; Bariain, C.; Goicoechea, J.; Elosua, C.; Hernaez, M.; Rivero, P.J.; Socorro, A.B.; et al. Optical Sensors Based on Lossy-Mode Resonances. *Sens Actuators B Chem* **2017**, *240*, 174–185, doi:10.1016/J.SNB.2016.08.126.
2. Chiavaioli, F.; Janner, D. Fiber Optic Sensing with Lossy Mode Resonances: Applications and Perspectives. *Journal of Lightwave Technology* **2021**, *39*, 3855–3870, doi:10.1109/JLT.2021.3052137.
3. Wang, Q.; Zhao, W.M. A Comprehensive Review of Lossy Mode Resonance-Based Fiber Optic Sensors. *Opt Lasers Eng* 2018, *100*, 47–60.

4. Fuentes, O.; Del Villar, I.; Corres, J.M.; Matias, I.R. Lossy Mode Resonance Sensors Based on Lateral Light Incidence in Nanocoated Planar Waveguides. *Scientific Reports 2019 9:1* **2019**, *9*, 1–10, doi:10.1038/s41598-019-45285-x.
5. Fuentes, O.; Corres, J.M.; Dominguez, I.; Del Villar, I.; Matias, I.R. Simultaneous Measurement of Refractive Index and Temperature Using LMR on Planar Waveguide. *Proceedings of IEEE Sensors* **2020**, *2020-October*, doi:10.1109/SENSORS47125.2020.9278727.
6. Dominguez, I.; Del Villar, I.; Fuentes, O.; Corres, J.M.; Matias, I.R. Dually Nanocoated Planar Waveguides towards Multi-Parameter Sensing. *Scientific Reports 2021 11:1* **2021**, *11*, 1–8, doi:10.1038/s41598-021-83324-8.
7. Dominguez, I.; Corres, J.M.; Fuentes, O.; Del Villar, I.; Matias, I.R. Multichannel Refractometer Based on Lossy Mode Resonances. *IEEE Sens J* **2022**, *22*, 3181–3187, doi:10.1109/JSEN.2022.3142050.
8. Sanchez, P.; Zamarreño, C.R.; Hernaez, M.; Matias, I.R.; Arregui, F.J. Optical Fiber Refractometers Based on Lossy Mode Resonances by Means of SnO2 Sputtered Coatings. *Sens Actuators B Chem* **2014**, *202*, 154–159, doi:10.1016/j.snb.2014.05.065.
9. Ascorbe, J.; Corres, J.M.; Del Villar, I.; Arregui, F.J.; Matias, I.R. Fabrication of Bragg Gratings on the End Facet of Standard Optical Fibers by Sputtering the Same Material. *Journal of Lightwave Technology* **2017**, *35*, 212–219, doi:10.1109/JLT.2016.2640021.
10. Gallego, E.E.; Ascorbe, J.; Del Villar, I.; Corres, J.M.; Matias, I.R. Nanofabrication of Phase-Shifted Bragg Gratings on the End Facet of Multimode Fiber towards Development of Optical Filters and Sensors. *Opt Laser Technol* **2018**, *101*, 49–56, doi:10.1016/J.OPTLASTEC.2017.11.001.
11. Pavlichenko, I.; Exner, A.T.; Guehl, M.; Lugli, P.; Scarpa, G.; Lotsch, B. v. Humidity-Enhanced Thermally Tunable TiO 2/SiO 2 Bragg Stacks. *Journal of Physical Chemistry C* **2012**, *116*, 298–305, doi:10.1021/jp208733t.
12. Wilkens, V.; Koch, C.; Molkenstruck, W. Frequency Response of a Fiber-Optic Dielectric Multilayer Hydrophone. *Proceedings of the IEEE Ultrasonics Symposium* **2000**, *2*, 1113–1116, doi:10.1109/ULTSYM.2000.921520.
13. Poxson, D.J.; Schubert, E.F.; Mont, F.W.; Kim, J.K.; Schubert, M.F.; Chhajed, S. Design of Multilayer Antireflection Coatings Made from Co-Sputtered and Low-Refractive-Index Materials by Genetic Algorithm. *Optics Express, Vol. 16, Issue 8, pp. 5290-5298* **2008**, *16*, 5290–5298, doi:10.1364/OE.16.005290.
14. Arregui, F.J.; Matias, I.R.; Cooper, K.L.; Claus, R.O. Fabrication of Microgratings on the Ends of Standard Optical Fibers by the Electrostatic Self-Assembly Monolayer Process. *Optics Letters, Vol. 26, Issue 3, pp. 131-133* **2001**, *26*, 131–133, doi:10.1364/OL.26.000131.
15. Chiavaioli, F.; Zubiate, P.; Del Villar, I.; Zamarreño, C.R.; Giannetti, A.; Tombelli, S.; Trono, C.; Arregui, F.J.; Matias, I.R.; Baldini, F. Femtomolar Detection by Nanocoated Fiber Label-Free Biosensors. *ACS Sens* **2018**, *3*, 936–943, doi:10.1021/acssensors.7b00918.
16. Rubin, M. Optical Properties of Soda Lime Silica Glasses. *Solar Energy Materials* **1985**, *12*, 275–288, doi:10.1016/0165-1633(85)90052-8.
17. Sultanova, N.; Kasarova, S.; Nikolov, I. Dispersion Properties of Optical Polymers. *Acta Phys Pol A* **2009**, *116*, 585–587, doi:10.12693/APHYSPOLA.116.585.
18. Imas, J.J.; Zamarreño, C.R.; Del Villar, I.; Matías, I.R. Optimization of Fiber Bragg Gratings Inscribed in Thin Films Deposited on D-Shaped Optical Fibers. *Sensors 2021, Vol. 21, Page 4056* **2021**, *21*, 4056, doi:10.3390/S21124056